Study of the Structure and Chemical Nature of Porous Si and Siloxene by STM, AFM, XPS, and LIMA

Shueh-Lin Yau, Mark Arendt, and Allen J. Bard*

Department of Chemistry and Biochemistry, The University of Texas at Austin, Austin, Texas 78712

Brian Evans

Microchemical Analysis and Surface Properties, Pilkington Technology Center, Lancashire, England

C. Tsai, J. Sarathy, and J. C. Campbell

Microelectronics Research Center, Department of Electrical and Computer Engineering, The University of Texas at Austin, Austin, Texas 78712

ABSTRACT

In situ scanning tunneling microscopy (STM) and *ex situ* atomic force microscopy (AFM) were used to examine the surface morphology of anodized p-Si(100) electrodes in F^--containing solutions. In addition to the formation of a mainly pitted and rough surface, *in situ* STM observation of anisotropic etching of Si(100) in dilute (1%) HF showed the formation of well-defined features, such as peninsulas, a 27 nm wide V-groove, and many protruding 5 nm wide micropyramids. High-resolution *in situ* STM resolved atomic features at the V-groove limiting (111) facets. Although this slightly etched Si sample contained no quantum pillars, it luminesced orange under UV irradiation, in the same way as a porous Si layer prepared by anodization in a more concentrated HF (1:1 HF:EtOH) solution. A loosely bound surface porous Si layer as thick as 100 nm was revealed by AFM and a 2 μm^2 square depression could be fabricated in this layer by exerting stronger compressive force. The chemical nature of the surface film prepared by anodic etching in 1:1 HF:EtOH was further probed by x-ray photoemission spectroscopy (XPS), transmission Fourier transform infrared spectroscopy (FTIR), and laser ionization microanalysis (LIMA) techniques. These results support the explanation that the photoluminescence from porous Si can be caused by a chemically modified (Si/H/O) layer on the surface (*e.g.*, a siloxene-type material).

Chemical and electrochemical etching of silicon has been applied to the fabrication of submicrometer features on the surface and the production of porous Si layers.[1] Because of the high porosity of porous Si, it can be oxidized readily in an O_2-rich environment to give a 1 μm thick dielectric SiO_2 layer for insulating electronic elements in integrated circuits.[2] Porous Si has also been suggested as a potential optical material for light emitting devices.[3] Preferential (anisotropic) etching of Si along the ⟨110⟩ and ⟨100⟩ directions is used in microfabrication.[4] A typical chemical etching solution for Si contains an oxidant to react with the surface Si atoms to form higher oxidation states, such as Si(II) and Si(IV), that react with F^- species to produce soluble complexes. The oxidizing strength of the oxidant plays a crucial role in determining the shape of the etched surface features. Too strong an oxidant, like nitric acid (HNO_3), leads to isotropic (orientation independent) etching.[5] Chemical etching of Si with an aqueous KOH solution is strongly anisotropic; this solution has been used to produce high aspect ratio surface features.[4] Generally speaking, the etch rate of Si follows the order of ⟨100⟩ > ⟨110⟩ > ⟨111⟩.[4] The mechanism and causes of this anisotropic etching are of interest and have been studied in attempts to improve Si micromachining capabilities.[6,7] One tentative model[4] involves correlating the dangling bond density on each of the low index Si surfaces with their reactivities, but the result failed to account for the marked difference in etch rate of 600:300:1 in 44 weight percent (w/o) KOH for the (100):(111):(110) planes whose dangling bond density ratio is only 1:0.58:0.71. Kendall[4] suggested that the growth of a passive oxide film on the (111) face is faster than the other two faces,[8] thus causing a different etching rate. However, others[9] claimed no oxide is produced during the etching reaction, and the difference was attributed to the orientation of dangling bonds, which profoundly affects the activation energy for the etching reaction. Recently, *in situ* scanning tunneling microscopy (STM) was applied to study etching of Si(111) in NaOH solution, and a potential dependent etching mechanism and an etching rate were proposed.[10]

* Electrochemical Society Life Member.

Mechanistic studies of porous Si formation have been conducted on the photoassisted dissolution of n-type Si[11] and p-type Si[12] in F^--containing solutions. For the former case, the dopants (*e.g.*, P) form positively charged centers, like $P^{\oplus}$, and are proposed to create microelectric fields in the depletion layer, which effectively trap the HF and holes at these local sites.[13] Si at these local reaction sites with higher field strengths consumes four holes, and this leads to a higher etching rate. For the latter case, dissolution of Si proceeds through the tunneling and thermionic emission mechanisms for heavily and lightly doped Si, respectively.[14] The doping density has a pronounced effect on the structure of the porous Si layer, as revealed by scanning electron microscope (SEM) results.[14]

We report here a high resolution *in situ* STM study of the surface morphology of a p-type Si(100) electrode before and after anodization in 1% HF. Anodic dissolution of p-Si in dilute HF was found to be anisotropic, and the STM revealed distinct surface features, such as a V-shaped trench. Two possible etching mechanisms of Si under our experimental conditions, which involved the simultaneous dissolution of Si at different rates, are proposed. These two reaction mechanisms dissolve Si at different locations to result in distinct Si surface morphology. Our STM data are consistent with the hole-tunneling model, which predicts a faster etching rate at the tips of pores than on a planar surface.[11c] Atomic features were discerned by STM on the smooth (111) side walls that confined the 70° V-groove. Although anisotropic etching can be implemented by other means, such as laser-induced reactive ion etching,[15] electrochemical etching of Si has the advantage of low cost, while producing better defined trench structures,[16] when compared to the bottle-shaped trenches formed by reactive ion etching.[17] We also tried to image lightly doped Si, but failed in this case to obtain a stable STM image, mainly because electron tunneling was inhibited due to the formation of a sufficiently wide depletion layer at the Si surface.

Porous Si prepared by anodic dissolution or chemical etching in a F^--containing solution has been of much interest recently, because of its intriguing visible photoluminescence and potential applications (*e.g.*, in electroluminescent devices).[3] While there have been numerous publica-

spective peak areas and VG elemental sensitivity factors. Correction of x-ray induced charging of each sample was accomplished by referencing the aliphatic C1s binding energy to 284.6 eV.[27] The binding energy was measured at the centroid of each individual peak and was then charge corrected. The powder samples of siloxene and anodized porous Si (scraped from the electrode surface) were prepared by depositing a slurry onto an In foil and evaporating the solvent. The HF dipping experiment was done by soaking a porous Si sample in 50% HF for 30 s in a nitrogen-filled box. The sample was then transferred to the UHV chamber after a thorough rinse with distilled water. Etched and unetched Si wafers were used directly without further processing. The resolution of the spectrometer was determined from a sputtered gold standard and was 1.45 eV FWHM at 50 eV pass energy.

Laser ionization microprobe mass spectrometry.—The LIMA-4A (Cambridge Mass Spectrometry Ltd., Cambridge) is capable of performing microanalysis in the transmission mode for thin samples or by using a reflection geometry for thick specimens. The instrument employs a time-of-flight (TOF) mass spectrometer, which allows detection of both positive and negative ions. The laser source, a Nd:YAG solid-state laser in an oscillator-amplifier combination, gives 1064 nm laser light, which can be quadrupled to the UV wavelength of 266 nm. This instrument provides the advantage of high lateral resolution of the sampled surface onto which a laser spot as small as 2 μm can be focused. The maximum laser powder can reach 10^{11} W cm^{-2}). In the present experiments, the power density was kept low (10^{9} W cm^{-2}) and the sample depth was restricted to a surface region of 4 to 100 nm deep.

Results and Discussion

In situ imaging during anodization of p-Si(100) in 1% HF.—The cyclic voltammetry of Si was consistent with the reported results for p-Si(100) electrodes in dilute HF.[11] A dilute (1%) HF solution was used only in the STM experiments to avoid attack of the STM head components. A bias voltage of 430 MVP ($E_{Si} = -0.73$ V *vs.* NHE; $E_{tip} = -0.30$ V *vs.* NHE) and a 2 nA feedback current were used to implement STM imaging in the constant height mode (Fig. 1). Stable STM imaging commenced immediately after the tip started scanning; however, some artifactual horizontal scan lines appeared initially. These are probably due to an initial 1.5 nm thick native dielectric SiO_2 layer on the Si, which is removed by exposure to the HF, leaving a Si surface terminated with hydrogen. Furthermore, as the p-Si electrode was under cathodic bias, electrons tunneled from the valence band of the p-Si into unoccupied states of the W tip. Tunneling out of p-Si was smaller, and resolution was lost when the Si potential was swept positive to -0.20 V (while maintaining a constant tip-substrate bias). At this potential, Si dissolution via a Si(II) valence state is expected.[11] The loss of resolution may also be by oxidation of the Si surface to produce a poorly conductive hydroxide or oxide film. When the Si potential was swept back to -0.73 V, the anodic oxide was removed by HF and the STM imaging sharpened again. The STM clearly revealed a local-layered-type surface morphology (Fig. 2) on the originally flat Si (100) electrode. The step height between two layers was *ca.* 1.6 nm, which corresponds to a depth of four layers. Parallel trenches appear in the ⟨110⟩ direction, cut into each terrace. These features suggest a layer-by-layer etching mechanism for the (100) face, in contrast to the step flow mechanism for the (111) surface.[28] Higher resolution STM scans of the trenches revealed a local V-groove feature defined by two 5 nm high pyramidal-shaped hills (Fig. 3). For better viewing, the image is rotated 90° clockwise with respect to the direction in Fig. 2. Many smaller pyramidal protrusions (approximately 5 nm wide and 2 nm high) are noticeable at the top and the bottom of the hills. The two side walls appear very clean, but some debris was seen at the bottom of the groove. The V-groove feature can be explained by the "self-stopping" nature of anisotropic etching on Si(100). As the etching fronts cut into the wafer along two ⟨110⟩ directions, they stopped at the point when the surface area of the (100) plane at the bottom of the groove was reduced to zero. However, our STM results seem to indicate that preferential dissolution of Si took place at the foot, rather than the top, of the hill where two ⟨110⟩ rows of Si atoms intersected (see Fig. 4). This can be explained by the higher hole tunneling efficiency and higher current flow at the tip of the pores. As the reaction continued, the etchant, presumably HF in this case, attacked Si upward and led to discontinuous strings of Si atoms, seen in the middle of the atomic image (Fig. 5). Before an entire row of Si atoms was removed, HF molecules already started to attack the next row of Si atoms and resulted in atomically flat (111) microfacets and a layered-type structure. The STM image indicates that the trench is 27 nm wide and *ca.* 5 nm deep. The theoretical depth of the trench, *ca.* 19 nm, was not faithfully revealed, because the blunt shape

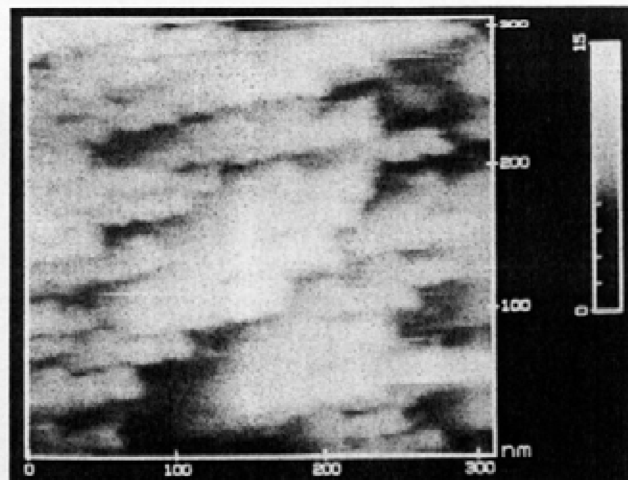

Fig. 2. STM topographic image of a Si(100) electrode after anodization. The image was collected at $E_{Si} = -0.73$ V, $E_{tip} = -0.33$ V, and $I_{tip} = 2$ nA. 50 nm long trenches cut through each terrace, leading to the formation of equal sized peninsulas running along the ⟨110⟩ direction. The step height was roughly 4.5 nm, as measured by the STM.

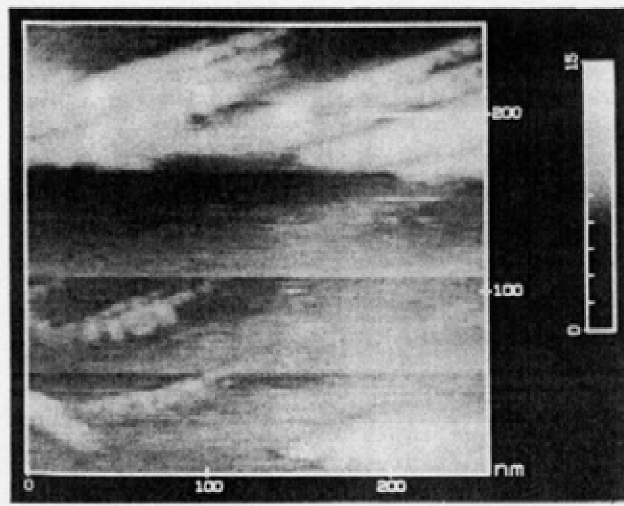

Fig. 1. *In situ* STM constant current image obtained at $E_{Si} = -0.73$ V, $E_{tip} = -0.30$ V, and $I_{tip} = 2$ nA. The image was collected 30 s after the HF solution was added to the cell so that most of the native surface oxide was probably already saturated with hydrogen adatoms. The elongated protruding stripes are attributed to polished damages.

spective peak areas and VG elemental sensitivity factors. Correction of x-ray induced charging of each sample was accomplished by referencing the aliphatic C1s binding energy to 284.6 eV.[27] The binding energy was measured at the centroid of each individual peak and was then charge corrected. The powder samples of siloxene and anodized porous Si (scraped from the electrode surface) were prepared by depositing a slurry onto an In foil and evaporating the solvent. The HF dipping experiment was done by soaking a porous Si sample in 50% HF for 30 s in a nitrogen-filled box. The sample was then transferred to the UHV chamber after a thorough rinse with distilled water. Etched and unetched Si wafers were used directly without further processing. The resolution of the spectrometer was determined from a sputtered gold standard and was 1.45 eV FWHM at 50 eV pass energy.

Laser ionization microprobe mass spectrometry.—The LIMA-4A (Cambridge Mass Spectrometry Ltd., Cambridge) is capable of performing microanalysis in the transmission mode for thin samples or by using a reflection geometry for thick specimens. The instrument employs a time-of-flight (TOF) mass spectrometer, which allows detection of both positive and negative ions. The laser source, a Nd:YAG solid-state laser in an oscillator-amplifier combination, gives 1064 nm laser light, which can be quadrupled to the UV wavelength of 266 nm. This instrument provides the advantage of high lateral resolution of the sampled surface onto which a laser spot as small as 2 μm can be focused. The maximum laser powder can reach 10^{11} W cm^{-2}). In the present experiments, the power density was kept low (10^9 W cm^{-2}) and the sample depth was restricted to a surface region of 4 to 100 nm deep.

Results and Discussion

In situ imaging during anodization of p-Si(100) in 1% HF.—The cyclic voltammetry of Si was consistent with the reported results for p-Si(100) electrodes in dilute HF.[11] A dilute (1%) HF solution was used only in the STM experiments to avoid attack of the STM head components. A bias voltage of 430 MVP ($E_{Si} = -0.73$ V *vs.* NHE; $E_{tip} = -0.30$ V *vs.* NHE) and a 2 nA feedback current were used to implement STM imaging in the constant height mode (Fig. 1). Stable STM imaging commenced immediately after the tip started scanning; however, some artifactual horizontal scan lines appeared initially. These are probably due to an initial 1.5 nm thick native dielectric SiO_2 layer on the Si, which is removed by exposure to the HF, leaving a Si surface terminated with hydrogen. Furthermore, as the p-Si electrode was under cathodic bias, electrons tunneled from the valence band of the p-Si into unoccupied states of the W tip. Tunneling out of p-Si was smaller, and resolution was lost when the Si potential was swept positive to −0.20 V (while maintaining a constant tip-substrate bias). At this potential, Si dissolution via a Si(II) valence state is expected.[11] The loss of resolution may also be by oxidation of the Si surface to produce a poorly conductive hydroxide or oxide film. When the Si potential was swept back to −0.73 V, the anodic oxide was removed by HF and the STM imaging sharpened again. The STM clearly revealed a local-layered-type surface morphology (Fig. 2) on the originally flat Si (100) electrode. The step height between two layers was *ca.* 1.6 nm, which corresponds to a depth of four layers. Parallel trenches appear in the ⟨110⟩ direction, cut into each terrace. These features suggest a layer-by-layer etching mechanism for the (100) face, in contrast to the step flow mechanism for the (111) surface.[28] Higher resolution STM scans of the trenches revealed a local V-groove feature defined by two 5 nm high pyramidal-shaped hills (Fig. 3). For better viewing, the image is rotated 90° clockwise with respect to the direction in Fig. 2. Many smaller pyramidal protrusions (approximately 5 nm wide and 2 nm high) are noticeable at the top and the bottom of the hills. The two side walls appear very clean, but some debris was seen at the bottom of the groove. The V-groove feature can be explained by the "self-stopping" nature of anisotropic etching on Si(100). As the etching fronts cut into the wafer along two ⟨110⟩ directions, they stopped at the point when the surface area of the (100) plane at the bottom of the groove was reduced to zero. However, our STM results seem to indicate that preferential dissolution of Si took place at the foot, rather than the top, of the hill where two ⟨110⟩ rows of Si atoms intersected (see Fig. 4). This can be explained by the higher hole tunneling efficiency and higher current flow at the tip of the pores. As the reaction continued, the etchant, presumably HF in this case, attacked Si upward and led to discontinuous strings of Si atoms, seen in the middle of the atomic image (Fig. 5). Before an entire row of Si atoms was removed, HF molecules already started to attack the next row of Si atoms and resulted in atomically flat (111) microfacets and a layered-type structure. The STM image indicates that the trench is 27 nm wide and *ca.* 5 nm deep. The theoretical depth of the trench, *ca.* 19 nm, was not faithfully revealed, because the blunt shape

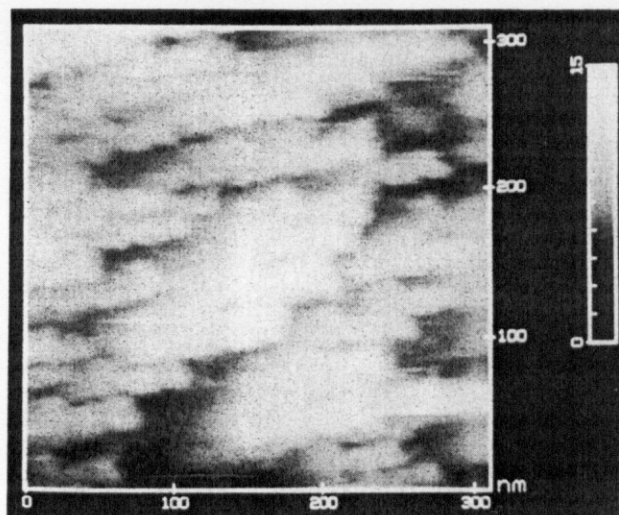

Fig. 2. STM topographic image of a Si(100) electrode after anodization. The image was collected at $E_{Si} = -0.73$ V, $E_{tip} = -0.33$ V, and $I_{tip} = 2$ nA. 50 nm long trenches cut through each terrace, leading to the formation of equal sized peninsulas running along the ⟨110⟩ direction. The step height was roughly 4.5 nm, as measured by the STM.

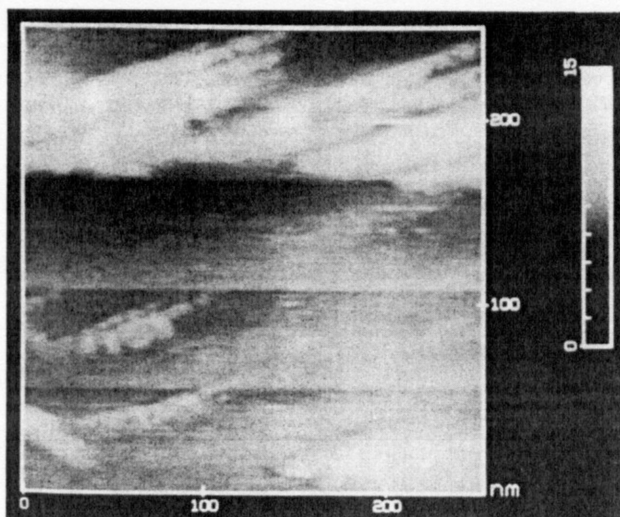

Fig. 1. *In situ* STM constant current image obtained at $E_{Si} = -0.73$ V, $E_{tip} = -0.30$ V, and $I_{tip} = 2$ nA. The image was collected 30 s after the HF solution was added to the cell so that most of the native surface oxide was probably already saturated with hydrogen adatoms. The elongated protruding stripes are attributed to polished damages.

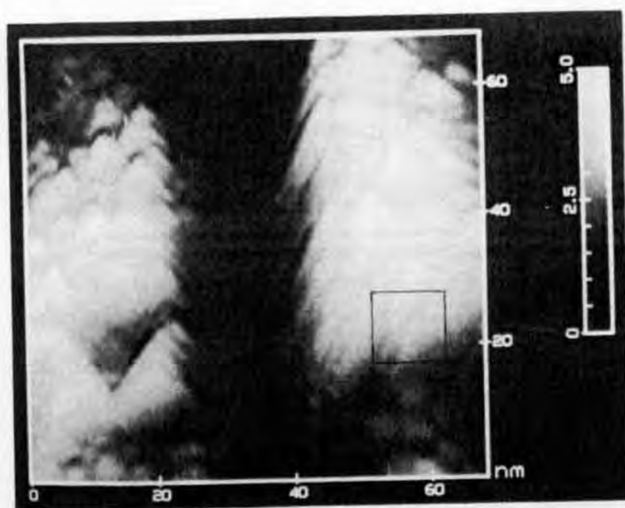

Fig. 3. STM topographic image showing the V-groove feature resolved from the trenches. This feature is a signature of anisotropic etching of Si(100). The image was collected at $E_{Si} = -0.73$ V, $E_{tip} = -0.58$ V, and $I_{tip} = 10$ nA. The V-groove is 27 nm wide and 5 nm deep, and the side walls, (111) planes, form a 70° angle, which is equal to those of the pyramids. The image was rotated 90° clockwise for a better view of this feature.

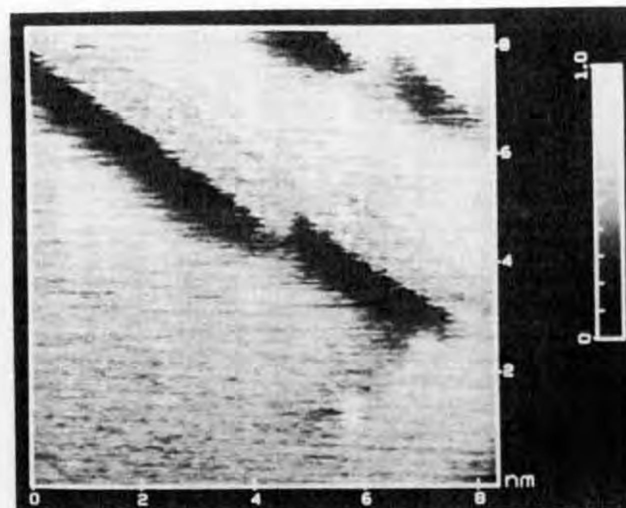

Fig. 5. High resolution STM image obtained from the region marked with a square box in Fig. 3. The image was obtained with 0.15 V bias voltage ($E_{Si} = -0.73$ V, $E_{tip} = -0.58$ V) and 10 nA tip current. The shadow following each terrace is a tracking error.

of the tip prevented it from dropping into the groove as it scanned across the depressed area. Even higher resolution STM scans allowed direct observation of atomic features (Fig. 5) at the side walls indicated by the box drawn in Fig. 3. The closest spacing between two rows of atoms, 0.40 nm, is close to the ideal value of 0.385 nm for the (1 × 1):H-phase of a Si(111) surface. The apparent shadows following each step-edge are due to the tip's tracking errors, caused by the slow response of the feedback loop as the tip scans from a high to a low area.

The different Si surface morphologies, revealed by the *in situ* STM, imply several concurrent Si etching reactions, such as those given in Eq. 1 and 2.

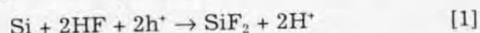

$$Si + 2HF + 2h^+ \rightarrow SiF_2 + 2H^+ \quad [1]$$

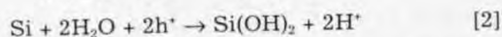

$$Si + 2H_2O + 2h^+ \rightarrow Si(OH)_2 + 2H^+ \quad [2]$$

In both cases Si dissolves through the capture of two holes, followed by reaction with HF and H_2O. Because the concentration of H_2O is two orders of magnitude higher than that of HF in the present case, the second reaction would tend to dominate. Ultimately, the etching rate is determined by the supply of holes from the bulk.[11] However, Si dissolution via a tetravalent state cannot be ruled out. The fact that trench features on a Si(100) wafer can be fabricated with an alkaline solution[4] suggests that the second pathway, which produces a $Si(OH)_2$ intermediate, can be responsible for the trench and pyramid features, while the first reaction might preferentially occur at surface defects like steps and kinks. Furthermore, *in situ* STM has revealed some regions on Si with no well-defined features. Possibly, Si(II) intermediates disproportionate to produce Si(IV) and Si(0), as suggested by Memming *et al.*[11a] and supported by *in situ* IR measurements.[29] While the Si(IV) species dissolve in the solution, the neutral Si will deposit back on the surface, and these Si deposits could react with HF, H_2O, and other Si neutral species. This mechanism might then produce the bluish thin film on the Si wafer which glowed weakly in the orange region under a handheld UV lamp similar to that of the porous Si.

AFM imaging of porous Si.—Although the AFM investigation of the nanostructures of porous Si has already been reported elsewhere,[30] we carried out additional studies to illustrate the presence of a loosely bound surface porous Si layer on top of the columnlike porous Si. Figure 6 shows a 15 μm^2 AFM image (in air) of the surface of a porous Si sample prepared by electrochemically etching Si in a concentrated HF solution for 5 min. The surface shows some

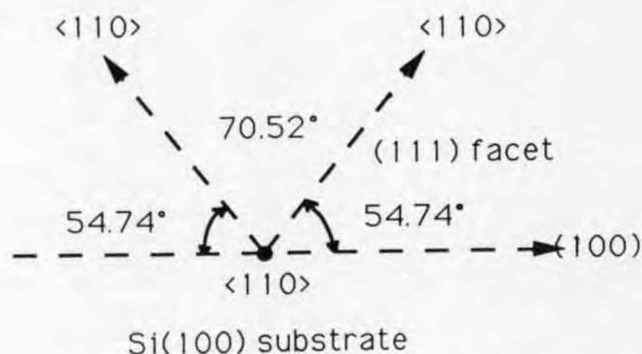

Fig. 4. A diagram to illustrate the V-groove surface features found in Fig. 3. The V-shape, which opens to 71°, is defined by the two (111) facets.

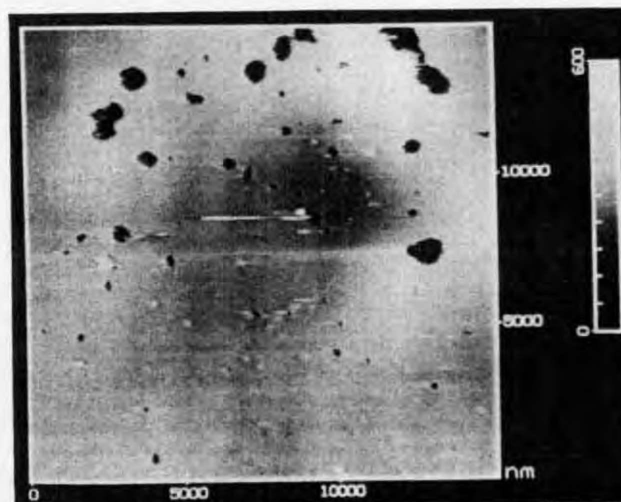

Fig. 6. AFM image of an anodized Si(100) sample. The Si wafer was prepared by constant current (5 mA cm^{-2}) etching for 5 min in 1:1 HF:EtOH solution.

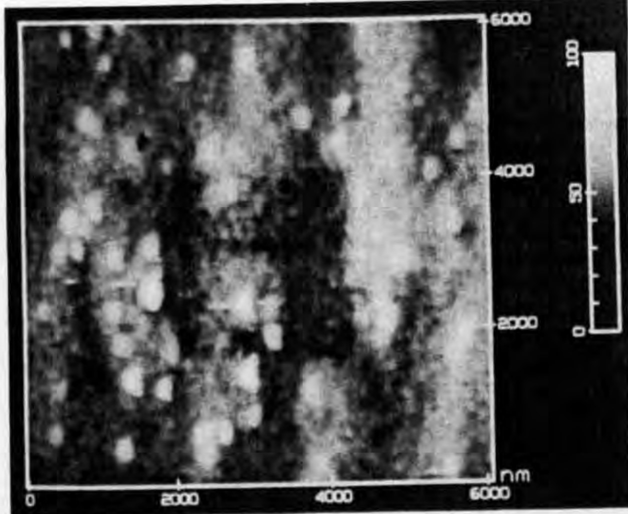

Fig. 7. AFM image of an anodized Si(100) wafer. The etching conditions were the same as for the sample in Fig. 6 except the etching time was 30 min. A 2 μm × 2 μm square depression was fabricated by increasing the imaging force.

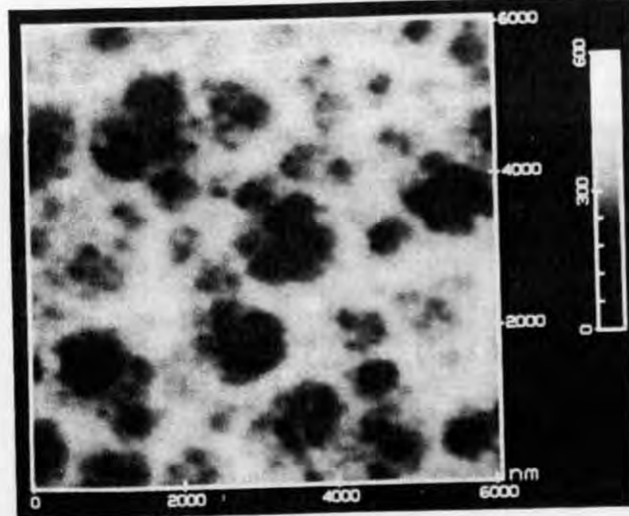

Fig. 8. AFM image of KOH-treated porous Si. The image was obtained on the same Si wafer as that in Fig. 7. The pore structure is clearly resolved by the AFM.

randomly distributed pits as well as an area of 100 nm^2 where the roughness is less than 3 nm. This sample produced orange photoluminescence, although the surface was rather flat and no quantum structures were seen. The lateral dimension of the pits varied between 0.1 μm and 1.5 μm, which represent the convolution of the tip size and sample morphology. Formation of pits suggests the presence of nucleation sites, *e.g.*, surface defects or impurity centers, where there are higher local dissolution rates of Si. The existence of pits of different sizes indicates that nucleation occurs throughout the 5 min etching period, rather than only initially. The AFM tip-sample interaction could be used to modify the surface morphology.[31] For example, a square depression could be formed on an etched Si surface by scanning a 2 μm by 2 μm region at a higher force (10^{-9} N) for 5 min (Fig. 7). The Si sample in Fig. 7 was anodized for a longer period (30 min), so that a much rougher surface (compared to that in Fig. 6) was produced. This result suggests the presence of a loosely attached amorphous Si film at the near-surface region, as reported by others.[32] On the other hand, Cullis and Canham[3c] and Cole *et al.*[33] have reported nanometer-scale crystallites in the surface coating. These differences may be due to differences in the way the Si samples were prepared.[32] The smallest surface features (20 nm^2) in Fig. 7 are still much larger than those expected for quantum confinement (<5 nm^2). It would be interesting to raster a high-resolution laser across the depressed region to measure the photoluminescence spectrum of this mechanically modified surface.

Both the anodized and chemically etched porous Si reacted rapidly with an aqueous alkaline (1*M* KOH) solution to generate hydrogen. After this reaction, the porous Si surface had turned whitish and the luminescence from the porous Si disappeared. An AFM scan of the KOH-etched Si wafer is shown in Fig. 8. Pores with a wide range of sizes, from 0.1 to 1 μm, and with apparent depths of 0.06 to 0.18 μm are observed. The roughness of this surface is apparently higher than that in Fig. 6, and yet, the latter emitted light, while the KOH-etched Si did not. Surface roughness and the pore structures thus do not appear to be the key factors in the production of photoluminescence from anodized Si. As shown below, Si/H/O chemical species formed on anodization are likely contributors to photoluminescence.

X-ray photoelectron spectroscopy.—Figure 9 shows the XPS results of the Si_{2p} binding energy of several Si specimens: (a) a native oxide on Si(100); (b) HF-dipped Si prepared by chemical etching; (c) chemically etched Si; (d) porous Si powder; and (e) siloxene prepared from $CaSi_2$. Spectrum a exhibits a prominant peak at 99.0 eV and a weak feature at 103.0 eV, which are associated with low valence (Si-Si) and high valence (SiO_2) Si species, respectively.[26] Spectra b and c were obtained for chemically etched Si; the sample used in b was treated with 49% HF for 30 s in a nitrogen-saturated environment before transfer into the UHV chamber and pumping to 10^{-10} Torr. The marked difference between these two samples is the diminished high valence Si signal in b, indicating that this HF-dipping procedure effectively removed silicon oxide to a level undetectable by XPS. This porous Si sample did not luminescence following this brief HF treatment. Although there was still roughly 4% oxide, as estimated from the O_{1s} spectrum (not shown), it is exclusively related to the carbon

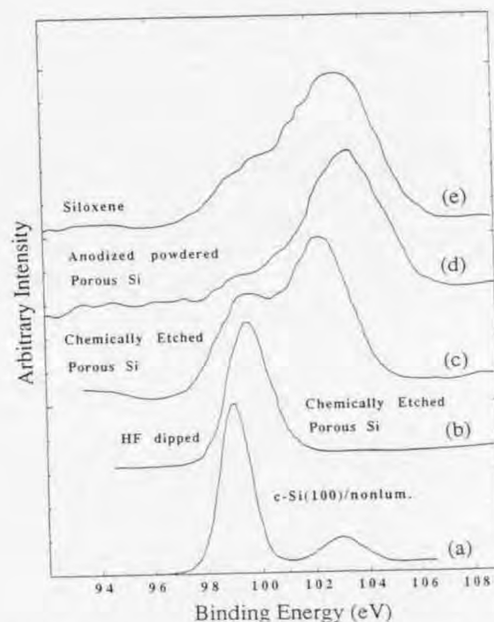

Fig. 9. XPS results for (a) the unetched Si(100); (b) chemically etched Si after dipping in 49% HF for 30 s; (c) chemically etched Si; (d) powder scraped from anodized Si, which was etched in HF:EtOH (1:1 by volume) with 5 mA cm^{-2} current density for 15 min; and (e) siloxene powder prepared by the procedure given in Ref. 24. The upshifts of the Si_{2p} state for samples (d) and (e) are attributed to the charging effect.

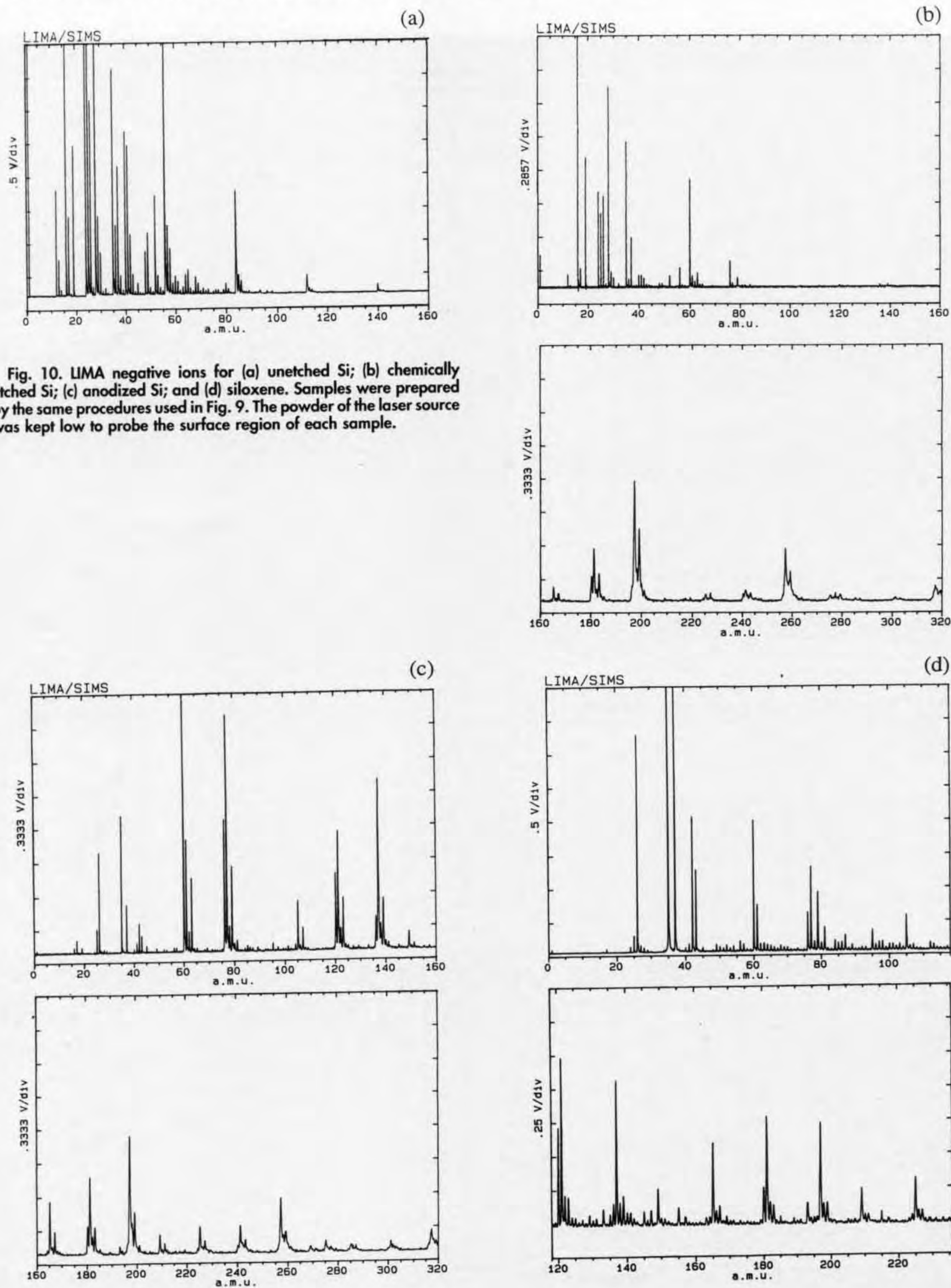

Fig. 10. LIMA negative ions for (a) unetched Si; (b) chemically etched Si; (c) anodized Si; and (d) siloxene. Samples were prepared by the same procedures used in Fig. 9. The powder of the laser source was kept low to probe the surface region of each sample.

contamination. In addition, the binding energy of Si_{2p} at 99.0 in b has shifted positive by 0.6 eV, due to an HF dipping induced silicon dihydride species.[34] An HF dipping experiment reported previously[35] was said not to quench photoluminescence from porous Si. However, the previous result was obtained with a very short (1 s) HF dip in an ambient (air) environment, so it is possible that some oxide still remained on the Si wafer surface. No XPS data were re-

ported in this experiment.[35] In a previous study, we showed that chemically etched Si and anodized Si exhibited different chemical reactivities toward HNO_3. Specifically, anodized Si reacted violently with HNO_3 while the chemically etched Si did not.[19b] Both Si specimens exhibited chemiluminescence upon contact with 4*M* HNO_3. A comparison of the XPS results of the chemically etched Si sample (b) and anodized porous Si in Fig. 5 of Ref. 30 shows a more intense (33 *vs.* 23 atomic percent) oxide feature for the chemically etched Si. This comparison implies that the anodized Si could have a higher hydrogen content in the film and thus a higher reducing strength. Silicon hydrides are known to be highly reactive; they catch fire or explode in air.[36] Our FTIR data (not shown here) provides good evidence for a reaction between HNO_3 and Si-H, because the 2108 cm^{-1} peak, which is associated with the Si-H stretch,[37] was diminished after the reaction.

The similarity between the properties of anodized Si and siloxene, a two-dimensional corrugated material containing O and H with a hexagonal Si ring structure, has already been pointed out.[19] The XPS results further support this similarity. As indicated by curves (d) and (e) in Fig. 9, the XPS results for both powder samples (siloxene and porous Si) show broad high valence Si states peaking at 103.4 eV, with a small contribution from low valence Si states. The high intensity of the low valence Si state for the siloxene sample indicated more Si-Si linkages than in the anodized Si powder. On the other hand, as indicated by a valence band spectroscopic study of porous Si,[18b] the crystallinity of porous Si in the film is not important in the photoluminescence. Amorphous porous Si photoluminesces; this also seems to be valid for siloxene. The siloxene photoluminescence spectrum red shifted (from 550 to 680 nm) upon annealing in vacuum while an order-disorder phase transition was noticed simultaneously.[38]

Laser ionization microanalysis.—Figure 10 shows the negative ion mass spectra obtained by LIMA for several different Si specimens: (a) untreated; (b) chemically etched; (c) anodized; and (d) siloxene. The peaks were identified by comparison to similar previous studies of a variety of Si-containing samples with the same apparatus. Most of the peaks for the ions with m/e less than 60 can be attributed to surface carbonaceous contamination, except for the peaks at m/e 28, 56, and 84, which represent Si^-, Si_2^-, and Si_3^-, respectively. The intense peak at m/e 60 represents SiO_2^-. Elemental silicon clusters are observed for the clean Si sample, but not for any of the etched Si ones. The major features between m/e 160 and 200 all appear in spectra (b), (c), and (d), suggesting a correspondence of the etched Si and siloxene. The peaks at m/e 197 (Si_3O_7H), 181 (Si_3O_6H), 165 (Si_3O_5H), 137 (Si_2O_5H), 121 (Si_2O_4H), 105 (Si_2O_3H), and 77 (SiO_3H) all correspond to $Si_nO_{2n-1}H$ $Si_nO_{2n}H$, or $Si_nO_{2n+1}H$ species. The assignments of these peaks are supported by the ratios of the Si isotopes[39] (Si^{28}:Si^{29}:Si^{30} = 92.23:4.67:3.10). All of these ions contain only one hydrogen atom, suggesting that these cluster ions arise from post laser ion-molecule reactions (hydrogen attachment) or fragmentation in the gas phase so that larger cluster ions were not observed in the mass spectrum. In addition, some cluster ions contain fluorine at m/e 63 (SiOF) and 79 (SiO_2F), indicating the presence of F on the surface of the etched Si samples.

Conclusions

The work reported here bears on the mechanism and surface structures formed upon anodization of Si and photoluminescence of etched Si. The *in situ* STM images reveal the anisotropic nature of the etching during the anodization of p-Si(100) in dilute HF, resulting in a V-shaped groove and many micropyramids. This technique is useful in microfabrication of Si wafers through control of current density and etching rate. The high-resolution STM images of a photoluminescent Si surface produced by etching did not show structures that could be described as quantum pillars. The nature of the Si surface species responsible for emission remains controversial. Broadly, at least three different kinds of structures have been proposed: pure Si quantum-features (pillars, dots), Si/H species, and Si/H/O (siloxene-type) species. There appears to be evidence that Si quantum-size structures[40] (other than anodically etched Si) show photoluminescence. An important factor in light emission from Si-based structures is the need to eliminate Si surface dangling bonds which can act as charge trapping and radiationless recombination centers and quench emission. For example, a hydrogenated amorphous Si film,[41] despite its high concentration of hydrogen in the matrix, carries a rather high dangling bond density (10^{16} cm^{-3}) and does not emit visible light at room temperature. However, reacting the film with oxygen ties up the dangling bonds, promoting an orange emission from the Si film at 298K.[41] Recently, the effect of oxygen on the photoluminescence of silicon materials has been described by Saunders *et al.*[42] and Rückschloss *et al.*[43] These two groups have independently demonstrated that vacuum-prepared quantum dots and hydrogenated amorphous Si do not emit light unless they are intentionally dosed with oxygen. These results, although obtained for silicon material prepared by a very different process than anodization, contrast with earlier reports of van Buuren *et al.*,[44] Vasquez *et al.*,[18b] and Zhang *et al.*,[45] who claim no oxygen is involved in photoluminescence from anodized silicon. A simple HF-dipping process for a porous Si surface provides a direct test for the role of oxygen. One finds that after the oxide is removed by HF, luminescence is quenched or markedly modified. However, orange luminescence recovers within minutes after the HF-etched Si wafer is let stand in air. Thus oxygen, either for surface-state capping or as a component of a surface compound, appears important in the luminescence of etched Si. Note that the presence of oxygen in a porous Si layer was previously demonstrated by secondary ion mass spectroscopy.[14] Morever, XPS and LIMA results show a strong correspondence between the etched Si specimens and siloxene samples, suggesting that the photoluminescence results from a surface layer on etched Si containing Si/O/H species.

Acknowledgments

This work was supported in part by a grant from the Office of Naval Research. We thank Huey Yang for help in IR measurements, Z. Guan for mass spectroscopy experiments, and I. Trachtenberg and Texas Instruments for generously providing the Si wafers. We also appreciate helpful discussions with P. McCord and F. R. Fan.

Manuscript submitted June 23, 1993; revised manuscript received Nov. 2, 1993.

The University of Texas at Austin assisted in meeting the publication costs of this article.

REFERENCES

1. (a) S. M. Sze, *Semiconductor Devices: Physics and Technology*, p. 428, John Wiley & Sons, Inc., New York (1985); (b) S. P. Murarka and M. C. Peckerar, *Electronic Material: Science and Technology*, p. 499, Academic Press, Ltd., London (1989).
2. (a) G. Bomchil, A. Halimaoui, and R. Herino, *Appl. Surf. Sci.*, **41/42**, 604 (1989); (b) L. G. Earwaker, M. C. Briggs, M. I. Nasir, J. P. G. Farr, and J. M. Keen, *Nucl. Instrum. Methods Phys. Res., Sect. B*, **56/57**, 855 (1991).
3. (a) L. T. Canham, *Appl. Phys. Lett.*, **57**, 1046 (1990); (b) A. Halimaoui, C. Oules, and G. Bomchi, *ibid.*, **59**, 304 (1991); (c) A. G. Cullis and L. T. Canham, *Nature*, **353**, 335 (1991).
4. (a) D. L. Kendall, *Ann. Rev. Mater. Sci.*, **9**, 373 (1979); (b) E. Bassous, *IEEE Trans. Electron Devices*, **ED-25**, 1178 (1978); (c) K. Bean, *ibid.*, **ED-25**, 1185 (1978).
5. D. L. Klein and D. J. D'Stefan, *This Journal*, **109**, 37 (1962).
6. (a) M. J. Declercq, L. Gerzberg, and J. D. Meindl, *This Journal*, **122**, 545 (1975); (b) A. Reisman, M. Berkenblit, S. A. Chan, F. B. Kaufman, and D. C. Green, *ibid.*, **126**, 1406 (1979).
7. (a) G. Stix, *Sci. Am.*, p. 106 (Nov. 1992); (b) C. D. Fung, P. W. Cheung, W. H. Ko, and D. G. Fleming, *Micromachining and Micropacking of Transducers*, Elsevier, Amsterdam (1985).

8. J. R. Ligenza, *J. Phys. Chem.*, **65**, 2011 (1961).
9. O. J. Glembocki, R. E. Stahlbush, and M. Tomkiewicz, *This Journal,* **132,** 145 (1985).
10. P. Allongue, H. Brune, and H. Gerischer, *Surf. Sci.*, **275,** 414 (1992).
11. (a) R. Memming and G. Schwandt, *Surf. Sci.*, **4,** 109 (1966); (b) M. J. Eddowes, *J. Electroanal. Chem.*, **280,** 297 (1990); (c) X. G. Zhang, *This Journal,* **138,** 3750 (1991); (d) C. Levy-Clement, A. Lagoubi, R. Tenne, and M. Neumann-Spallart, *Electrochim. Acta,* **37,** 877 (1992).
12. F. Gaspard, A. Bsiesy, M. Ligeon, F. Muller, and R. Herino, *This Journal,* **136,** 3043 (1989).
13. V. M. Dubin, *Surf. Sci.*, **274,** 82 (1992).
14. M. I. J. Beale, J. D. Benjamin, M. J. Uren, N. G. Chew, and A. G. Cullis, *J. Cryst. Growth,* **73,** 622 (1985).
15. C. Arnone and G. B. Scelsi, *Appl. Phys. Lett.*, **54,** 225 (1989).
16. V. Lehmann and H. Föll, *This Journal,* **137,** 653 (1990).
17. D. Chin, S. H. Dlaung, and G. J. Long, *ibid.*, **132,** 1705 (1985).
18. (a) C. Tasi, K. H. Li, J. Sarathy, S. Shih, J. C. Campbell, B. K. Hance, and J. M. White, *Appl. Phys. Lett.*, **59,** 2814 (1991); (b) R. P. Vasquez, R. W. Fathauer, T. George, A. Ksendzov, and T. L. Lin, *ibid.*, **60,** 1004 (1992).
19. (a) M. S. Brandt, H. D. Fuchs, M. Stutzmann, J. Weber, and M. Cardona, *Solid State Commun.*, **81,** 307 (1992); (b) P. McCord, S. L. Yau, and A. J. Bard, *Science*, **257,** 68 (1992).
20. P. Deák, M. Rosenbauer, M. Stutzmann, J. Weber, and M. S. Brandt, *Phys. Rev. Lett.*, **69,** 2531 (1992).
21. K. A. Littau, P. J. Szajowski, A. J. Muller, A. R. Kortan, and L. E. Brus, *J. Phys. Chem.*, **97,** 1224 (1993).
22. T. Unagami, *This Journal,* **127,** 476 (1980).
23. J. K. Sass, J. K. Gimzewski, W. Haiss, K. H. Besocke, and D. Lackey, *J. Phys. Condens. Matter.*, **3,** S121 (1991).
24. F. Kenny and R. B. Kurtz, *Anal. Chem.*, **22,** 693 (1950).
25. (a) Y. Sugawara, T. Ischizaka, and S. Morita, *J. Vac. Sci. Technol.*, **B9,** 1092 (1991); (b) Y. Kim and C. M. Lieber, *Science,* **257,** 375 (1992).
26. M. Chen, I. P. Batra, and C. R. Brundle, *J. Vac. Sci. Technol.*, **16,** 1216 (1979).
27. C. D. Wagner, W. M. Riggs, L. E. Davis, J. K. Moulchi, and G. E. Muilenberg, *Handbook of Photoelectron Spectroscopy,* p. 17, Perkin-Elmer Corp., Norwalk, CT (1979).
28. H. E. Hessel, A. Feltz, M. Reiter, U. Memmert, and R. J. Behm, *Chem. Phys. Lett.*, **186,** 275 (1991).
29. L. M. Peter, D. J. Blackwood, and S. Pons, *Phys. Rev. Lett.*, **62,** 308, (1989).
30. C. Tsai, K. H. Li, J. C. Campbell, B. K. Hance, M. F. Arendt, J. M. White, S. L. Yau, and A. J. Bard, *J. Electron. Mater.*, **21,** 995 (1992).
31. (a) S. L. Yau, T. P. Moffat, and A. J. Bard, *Chem. Phys. Lett.*, **198,** 383 (1992); (b) B. Parkinson, *J. Am. Chem. Soc.*, **112,** 7498 (1990).
32. (a) Y. Arita and Y. Sunohara, *This Journal,* **124,** 285 (1977); (b) T. George, M. S. Anderson, W. T. Pike, T. L. Lin, R. W. Fathauer, K. H. Jung, and D. L. Kwong, *Appl. Phys. Lett.*, **60,** 2359 (1992); (c) K. H. Jung, S. Shih, D. L. Kwong, T. George, T. L. Lin, H. Y. Liu, and J. Zarada, *This Journal,* **139,** 3363 (1992).
33. M. W. Cole, J. F. Harvey, R. A. Lus, D. W. Eckart, and R. Tsu, *Appl. Phys. Lett.*, **60,** 2800 (1992).
34. G. Grundner and H. Jacob, *Appl. Phys. A,* **39,** 73 (1986).
35. S. M. Prokes, W. E. Carlos, and V. M. Bermudez, *Appl. Phys. Lett.*, **61,** 1447 (1992).
36. J. D. Lee, *Concise Inorganic Chemistry,* 4 ed., p. 451, Chapman & Hall, Inc., New York (1991).
37. (a) P. Dumas and Y. J. Chabal, *Chem. Phys. Lett.*, **181,** 537 (1991); (b) P. Gupta, V. L. Colvin, and S. M. George, *Phys. Rev. B.*, **37,** 8234 (1988).
38. H. Ubara, T. Imura, A. Hiraki, I. Hirabayashi, and K. Morigaki, *J. Non-Cryst. Solids,* **59/60,** 641 (1983).
39. *CRC Handbook of Chemistry and Physics,* D. R. Lide, Editor, pp. 11-32, CRC Press, Boston, MA (1991).
40. W. L. Wilson, P. F. Szajowski, and L. E. Brus, *Science,* **262,** 1242 (1993).
41. (a) J. C. Knights, R. A. Street, and G. Lucovsky, *J. Non-Cryst. Solids,* **35/36,** 279 (1980); (b) R. Carius, R. Fischer, E. Holzenkämpfer, and J. Stuke, *J. Appl. Phys.*, **52,** 4241 (1981).
42. W. A. Saunders, P. C. Sercel, R. B. Lee, L. A. Atwater, K. J. Vahala, R. C. Flagan, and E. J. Escorcia-Aparcio, *Appl. Phys. Lett.*, **63,** 1549 (1993).
43. M. Rückschloss, B. Landkammer, and S. Veprek, *ibid.*, **63,** 1474 (1993).
44. T. van Buuren, Y. Gao, T. Tiedje, J. R. Dahn, and B. M. Way, *ibid.*, **60,** 3013 (1992).
45. Z. Zhang, M. M. Lerner, T. Alekel III, and D. A. Keszler, *Chem. Mater.*, **5,** 749 (1993).

Reprinted from Journal of the Electrochemical Society
Vol. 141, No. 2, February 1994
Printed in U.S.A.
Copyright 1994